Article type : Full Paper

Improved sensitivity and temporal resolution in perfusion FMRI using velocity selective inversion ASL

by

Luis Hernandez-Garcia, Ph.D.

Jon-Fredrik Nielsen, Ph.D.

Douglas C Noll, Ph.D

Running title: "Functional MRI using velocity selective inversion ASL"

Word count:

4,876 (manuscript only)

Corresponding Author:

Luis Hernandez-Garcia, Ph.D.

Research Professor

University of Michigan FMRI Laboratory

2360 Bonisteel Blvd.

Ann Arbor, MI 48109-2108

hernan@umich.edu

Abstract

Purpose

This work aims to investigate the utility of velocity selective inversion pulses for perfusion weighted functional MRI.

Methods

Tracer kinetic properties of velocity selective inversion (VSI) pulses as an input function for an arterial spin labeling (ASL) experiment were characterized in a group of healthy participants. Numerical simulations were conducted to search for a robust set of timing parameters for FMRI time series acquisition with maximal signal to noise ratio efficiency. The performance of three VSI pulse sequences with different timing parameters was compared to a pseudo-continuous ASL sequence in a simple FMRI experiment conducted on healthy participants.

Results

The fit to the tracer kinetic model yielded arterial CBV of 1.24 +/- 0.52% and 0.45 +/ 0.11% and perfusion rates of 60.8 +/- 32.3 and 34.4 +/- 5.4 ml/min/100g for grey and white matter, respectively. Bolus arrival times were estimated as 75.7 +/- 21 ms and 349 +/- 78 ms for grey and white matter, respectively.

The FMRI experiments showed that VSI pulses yield comparable sensitivity to PCASL with similar timing parameters (TR = 4 seconds). However, VSI pulses could be used at a faster acquisition speed (TR=3 seconds) and were more sensitive to neuronal activity than PCASL pulses, as evidenced by the 31% higher Z scores obtained on average in the active regions.

Conclusions

VSI pulses can be very beneficial for perfusion weighted functional MRI because of their tracer kinetic characteristics, which allow a faster acquisition rate while maintaining an efficient labeling input function.

Introduction

Arterial Spin Labeling (ASL) allows for quantitative imaging of perfusion without the use of exogenous tracers (1). In addition to baseline perfusion imaging, ASL techniques can also be used to carry out functional MRI experiments, as changes in perfusion are well known to be related to changes in brain activity. ASL-based FMRI is generally challenged by low signal to noise ratio (SNR), although it offers significant advantages in terms of its stability and its ability to produce a quantifiable measurement of a physiological parameter. Indeed, ASL based FMRI was found to be more stable across subjects than BOLD or even calibrated BOLD (2–4) and many longitudinal FMRI studies have used ASL acquisitions (for examples, see refs (5, 6, 7,8)).

Velocity and acceleration selective pulses have been recently shown to be an attractive option for ASL perfusion imaging because of potential gains in SNR and decreased sensitivity to bolus arrival time variations (9–14). While typical ASL labeling schemes target inflowing arterial blood spins based on their spatial position relative to the tissue of interest (e.g., pseudo-continuous ASL, or PCASL, pulses label spins as they cross a plane upstream of the tissue of interest), velocity selective labeling, on the other hand, targets moving spins regardless of their location. As a result, the time elapsed between the spins getting labeled and arriving at the capillary bed is virtually removed. Previous work has demonstrated that velocity selective saturation pulses can thus eliminate bolus arrival time effects (11). Furthermore, velocity selective *inversion* (VSI) pulses yield greater labeling efficiency (14,15). Since velocity selective labeling ASL can be potentially acquired faster than continuous ASL, this could result in an additional SNR boost. As a result, we hypothesize that VSI-based ASL acquisitions will produce images with SNR greater than PCASL, and with reduced sensitivity to arrival time variations.

Thus, one goal of this work was to test the utility of VSI pulses for perfusion-based functional brain imaging and to optimize the timing parameters of ASL image time series acquisition, which has not been previously investigated. The optimized ASL should achieve higher temporal resolution and higher SNR in ASL imaging, by collecting more images per unit time.

In this work, we first measured and characterized the uptake of the input function generated by VSI pulses experimentally. We aimed to verify theoretical predictions about the efficiency of the labeling pulses under experimental conditions and about the tracer kinetics model of the ASL signal generated by VSI pulses. We also aimed to obtain estimates of the width and amplitude of the input bolus in order to design the timing parameters of the FMRI sequence. We then tested the performance of VSI-ASL against the more standard PCASL method in a simple perfusion weighted FMRI experiment. We also compared different timing parameters for the VSI acquisition in order to investigate the sensitivity, SNR, and functional contrast-to-noise ratio (CNR) of the pulse sequence.

Methods

Characterization of the VSI input function: Experiments

In the first experiment, five healthy volunteers, aged between 40 and 56 were scanned using a 3T MR750 scanner (GE Medical Systems, Waukesha, WI) and a 32 channel receive-only coil (Nova Medical, Wilmington, MA). As depicted in Fig. 1, the acquisition scheme consisted of a 3D stack of spirals acquisition preceded by an ASL preparation as in (16). In this case the ASL preparation was done with a VSI pulse (15), a variable post labeling delay, and an optional velocity selective arterial saturation pulse for arterial suppression 50 ms before acquisition. No background suppression pulses were used. Label uptake curves were collected by varying the delay between labeling and acquisition, to estimate the following unknown parameters: (1) bolus arrival time, (2) perfusion rate, and (3) arterial blood volume fraction in both the grey and white matter.

The VSI pulses were generated using the method described by Qin et al [Qin 2016]. Specifically, The VSI pulses (see Supporting Fig. S1) consisted of a train of nine 20 deg hard pulse segments (81.25 mG for 160 us) separated by 6 ms gaps. Two refocusing hard pulses (117 mG for 1 ms) were inserted in those gaps with an MLEV phase pattern (14,17). Velocity encoding was done along the Z axis by inserting triangular gradient pulses (Gmax=2 G/cm, 300us ramp, 200us gap between pulses) of alternating sign between RF pulses. The non-selective case was carried out by using gradient pulses of the same sign. The total duration of the pulse train was 49.4 ms. The arterial suppression pulses were based on a symmetric BIR-8 velocity selective saturation scheme, as shown in Supporting Figure S2 (18,19). A Bloch simulation of the velocity profile of both of these pulses is shown on the right side of Supporting Fig. S3. The Bloch simulations used T1 of 1700 ms, and T2 of 150 ms (15,20). The velocity profiles of both pulses can be seen in greater detail in Supporting Figure S3. We note that the cutoff velocity for the velocity saturation pulse was set to 0.7 cm/s, and that the efficiency of the velocity selective inversion pulse varies with velocity, as expected. The theoretical mean labeling efficiency (defined as the magnetization difference between velocity selective and non-selective cases, relative to the relaxed magnetization) is 84% for the range between 5 and 80 cm/s.

The spiral image acquisition parameters were: matrix size = 128x128x16, voxel size = 0.18x0.18x0.6 cm, BW = 85 kHz, TR = 4000 ms, TE = 4.5 ms, nominal flip angle = 30 deg., No. interleaves = 2, No. of averages = 10 (5 control and 5 labeled), two dummy scans. The total scan time was 88 seconds.

In order to estimate the uptake rate of the VSI input function into the extravascular space and to characterize its shape, 13 images were collected with different post inversion delays from 200 to 2600 ms. with no arterial suppression. The experiment was then repeated with arterial suppression pulses (BIR-8 velocity selective saturation) turned on. No VSI or arterial suppression pulses were applied in the first two images of the time series, in order to collect reference

images. VSI pulses were applied in the remaining 8 images, alternating between selective and non-selective pulses.

Images were reconstructed, realigned and smoothed with a Gaussian kernel (full width at half max = 6 mm). The non-selective images at each post inversion delay were used to fit an inversion recovery curve and estimate the longitudinal relaxation rate, and the inversion efficiency of the VSI pulses in the stationary tissue. The resulting R1 maps were used to segment grey matter and white matter regions.

The ASL signal at each voxel was calculated as the percentage signal difference between the magnitudes of the selective and non-selective images, relative to the reference images (i.e., no prep. pulses). The average ASL signal as a function of the post inversion delay was calculated for white and grey matter separately for each subject.

Characterization of the VSI input function: Theory

A two-compartment model (vascular and extra vascular) of the ASL signal (without arterial suppression) was constructed to fit the observed data as a function of the post inversion delay, as follows (21,22). The extravascular compartment's longitudinal magnetization is described by a modified Bloch equation:

$$\frac{dM_z}{dt} = \left(M_z^0 - M_z(t)\right) \cdot R_1 + f \cdot M_a(t) - \frac{f}{\lambda} \cdot M_z(t) \quad [1]$$

where $M_z(t)$ and $M_a(t)$ are the longitudinal magnetization of tissue and arterial blood, respectively. R1 is the tissue's relaxation rate. Perfusion rate is captured by f, and λ is the blood:brain partition coefficient. The arterial compartment can be modeled by a simple inversion-recovery equation, following the VSI pulse:

$$M_a(t) = M_a^0(1 - 2 \cdot \alpha \cdot e^{-t \cdot R1_a}) \quad [2]$$

Here, α is the efficiency of the VSI pulse, and R_{1a} is the longitudinal relaxation rate of arterial blood. For the arterial blood, α was assumed to be 0.15 in the velocity selective case and 0.7 in the non-selective case.

In order to capture the bolus arrival time (BAT), defined as the time it takes the uninverted spins in the velocity selective case to reach the extra-vascular compartment, we modified the arterial magnetization input into the tissue, such that in the velocity selective case, the early part of the input is inverted, but after a delay, the non-inverted spins arrive into the tissue compartment. Thus, the arterial input function is made up of both inverted and un-inverted spins, in varying proportion. Specifically, the new arterial magnetization function is

$$M_a(t) = B(t) \cdot M_{a,sel}(t) + \big(1 - B(t)\big) \cdot M_{a,nonsel}(t) \qquad [3]$$

Where B(t) is the proportion of spins in the arterial compartment that is un-inverted by the VSI pulse. B(t) is a sigmoid function whose inflection point happens at the bolus arrival time. It was constructed by integrating a Gaussian distribution function, whose mean was the bolus arrival time, and its standard deviation was fixed to 100 ms., as an approximation of the distribution. Finally, the observed signal, $S(t)$, is a mix of the vascular and extravascular compartments. It can be written as

$$S(t) = CBV_a \cdot M_a(t) + (1 - CBV_a) \cdot M_z(t) \quad [4]$$

where CBV_a is the arterial blood volume fraction.

As in most ASL experiments, the VSI experiment consists of two acquisitions preceded by velocity selective and non-selective inversion pulses. In the non-selective case, the initial conditions for arterial and extravascular compartments are $M_a(0) = 1 - 2 \cdot \alpha$ and $M_z(0) = 1 - 2 \cdot \alpha_e$, respectively ($\alpha$ and α_e denote separate inversion efficiency for vascular and extravascular spins). In the velocity selective case, the arterial magnetization in the extravascular compartment is still inverted, but the arterial magnetization is "lightly" saturated by the VSI pulses and $M_a(0) \cong 1 - \alpha$.

We used a non-linear least squares algorithm to estimate (i) bolus arrival time (ii) perfusion rate, (iii) arterial blood volume fraction and (iv) arterial inversion efficiency from both grey and white matter using the unsuppressed uptake curves. We fixed the inversion efficiency of the arterial blood to 0.58 for the arterial spins for the white matter data, based on the grey matter results (we found that the white matter data were too noisy to fit all the parameters at once.

To reduce to problem size, we fixed the value of the inversion efficiency to the mean of the grey matter value). We assumed T1 relaxation of arterial blood to be 1700 ms (23).

Numerical Optimization of Timing Parameters

Using equations 1-4, we simulated the longitudinal magnetization in a voxel with the above VSI pulse sequence with multiple TRs (from 2-5 sec.), and post labeling delays (0.5-2 sec.) in order to design a VSI sequence for fast perfusion weighted FMRI that maximizes the SNR of the ASL signal for a given total imaging time. We used the same two-compartment model as before, and the following parameters, based on the estimates from the uptake curves above: perfusion rate = 60 ml/min/100g, arterial blood volume = 1 %, VSI bolus width = 2600ms, tissue T1 = 1400ms, arterial T1 = 1700 ms, inversion efficiency = 80%. We assumed that 3D image acquisition takes 600ms (experimentally, the acquisition time for 3D stack of spirals was 521 ms). Stationary spins were assumed to be completely saturated by the end of the image acquisition window. We used this framework to calculate the ASL signal (difference between selective and non-selective images). The relative SNR of the signal per unit of time was calculated by scaling the ASL signal by the square root of the number of images collected in that unit of time (or one over the square root of TR).

Eddy Current Tests

In a separate experiment, we tested the eddy current artefacts due to the VSI pulses described in the original implementation paper by Qin et al (24), by repeating the above uptake experiment on an FBIRN gel phantom (25). We examined the signal differences between velocity selective and non-selective acquisitions in terms of the differences introduced into the magnitude and the phase of the images. We calculated the root mean square phase and magnitude differences, separately, as a function of the post inversion delay.

FMRI experiments

Healthy subjects (N=6, ages from 40 to 56) were scanned using a 3.0T MR750 scanner. The subjects were instructed to tap their fingers of their right hand for 20 seconds while being stimulated with an 8Hz flashing checkerboard pattern. The stimulus was repeated 5 times, preceded by 40 seconds of inactivity (total time = 300 s). This experimental paradigm was repeated four times while the subjects were scanned with the following four ASL sequences, using parameters based on simulation: (1) PCASL labeling for 1600ms, followed by 1800 ms post inversion delay (PID), TR = 4000 ms; (2) VSI label followed by 1800 ms PID, TR = 4000 ms; (3) VSI label followed by 1800 ms PID, TR = 3000 ms; and (4) VSI label followed by 1200 ms, TR = 2000 ms. As before, acquisition in all four cases was done with a 3D stack of spirals sequence (64 x64 x 16 matrix, 0.344 x 0.344 x 0.6 cm voxel size). No background or arterial suppression pulses were used. Off resonance correction for the PCASL pulses was applied after a calibration experiment, as recommended in (26).

The time series was reconstructed, motion corrected, smoothed with 6 mm Gaussian kernel and surround-subtracted in time. Linear regression was used to detect and estimate stimulus related activation, including nuisance regressors identified using the CompCor technique (27). Z score maps corresponding to the activation were calculated from the resulting estimates. The number of voxels with a Z score greater than 3 within the brain were tabulated for each case.

Spatial noise was estimated as the standard deviation of the temporal mean magnitude of pixels outside the brain. Temporal noise was estimated as the temporal standard deviation averaged over all the pixels inside the whole brain (without removal of task or drift effects). Spatial and temporal SNR were defined as the mean ASL signal inside the brain divided by the spatial and temporal noise standard deviations, respectively. Contrast to Noise Ratio (CNR) can be inferred from the Z scores, which are derived from the T statistic; in this case, a ratio of the activation size estimate over the estimate of its variance and accounting for the number of measurements as degrees of freedom.

Results

Characterization of the VSI input function and pulse sequence optimization

Figure 2 shows the simulated longitudinal magnetization (Mz) of the arterial compartment and of the extravascular compartment following the VSI pulses, using the constants extracted from grey matter voxels in a representative subject. In the non-selective case, shown in the top panel, both the arterial and extravascular spins are inverted with 59% and 72% efficiency, respectively, and relax at their corresponding T1 rates of 1700 ms and 1400 ms, respectively. In the velocity selective case, shown in the middle panel, the arterial compartment is assumed to be tipped down only 15%. However, when acquiring images immediately after the inversion pulse, the signal is dominated by the slow moving spins in the extravascular compartment and in the arterioles, which are inverted by the pulse . There is a short delay before the un-inverted spins move into the arterioles, capillaries and extravascular space. Consequently, the model includes a delay (or "bolus arrival time") before the un-inverted spins entered the compartment. Finally, the ASL signal is shown in the bottom panel as the difference between the total magnetization in the selective and the non-selective cases. If the subtraction is performed using complex images, then its value should essentially reflect the concentration of labeled spins in the voxels as a function of the post inversion delay (shown in blue). Note, however, that ASL images are typically constructed by subtracting magnitude images and this results in the sign flip in the early part of the curve, before the labeled arterial spins have reached the null point of their recovery and still have negative longitudinal magnetization. This would rarely affect the use of VSI-ASL in practice, since post labeling delays are typically longer than 1s.

The same images from the uptake experiments (using variable post inversion delays) were first used to estimate T1 relaxation and inversion efficiency . The average T1 relaxation rates estimated from the unsubtracted, non-selective images as a function of the post inversion delay were 1475 +/- 11 and 892 +/- 22 ms for grey and white matter respectively. From the same

non-linear least-squares fit, the average inversion efficiency of the stationary tissue was 71.6 +/- 1.0 % and 73.9 +/- 1.9 % in the grey and white matter, respectively.

ASL images collected at different times after the VSI pulse can be seen in Fig. 3. ASL time courses as a function of the post inversion delay were extracted from grey and white matter, and averaged separately across all participants, as shown in Fig. 4. We note that early images after the VSI pulse clearly show the arterial network as a negative signal. We also note that the vasculature is not visually apparent (Fig. 3) when the arterial suppression pulse was used.

As predicted by simulations in Fig. 2, the ASL images have negative value initially, and the sign of the ASL image changes around between 600 and 800 ms after the inversion pulse. The ASL signal decays afterward. This is consistent with the labeling pulse inverting the magnetization in the arteries, which then relaxes back to the positive axis, and with the fact that the ASL images were calculated as a subtraction of magnitude images.

The proposed two-compartment model fit to the unsuppressed time courses can be seen in Fig. 5 (in agreement with the predicted curves in Fig. 2). The parameter estimates obtained from the fitting procedures are shown in Table 1 To summarize, the fit to the tracer kinetic model yielded arterial CBV of 1.2 +/-0.52 % and 0.45 +/ 0.11% and perfusion rates of 60.8 +/- 32.2 and 34.4 +/- 5.4 ml/min/100g for grey and white matter, respectively. Bolus arrival times were estimated as 75.6 +/- 21 ms and 349 +/- 77 ms for grey and white matter, respectively. The inversion efficiency in the arterial blood was estimated to be 59 +/- 8.8 % in the grey matter. This efficiency was assumed to be the same for the white matter compartment, as well.

Figure 6 shows the simulated evolution of the longitudinal magnetization of both the arterial and the extravascular compartments of a theoretical grey matter voxel, when imaged with a VSI perfusion weighted FMRI sequence time series (at rest). The arterial compartment is inverted by the non-selective pulses, but only partially tipped by the velocity-selective pulses. The extravascular compartment (stationary and slow moving spins) becomes inverted in both cases.

We also note that in our simulation model, the 3D image acquisition was assumed to saturate all the spins in the imaging slab, but that the arterial spins are replaced before the next labeling period. We calculated the expected ASL signal (% signal change) after two cycles, when the system reaches an equilibrium, and its relative SNR efficiency (the SNR within a fixed scanning period, or SNR per unit of time). Figure 7 shows the expected ASL signal (top two panels) and its SNR efficiency (bottom two panels) as a function of TR and post inversion delay. The left side shows the signals from the whole voxel, whereas the right side shows only the extravascular compartment (i.e., the case when arterial suppression pulses are used). We also point out that the black regions on the bottom left corner of the images correspond to unrealistic timing combinations (i.e., TR < PID + acquisition time) and were not included in the analysis. These simulations predict that, under ideal assumed conditions, optimal SNR efficiency occurs at TR = 2.75 s and PID of 0.5 s when no arterial suppression is used. The optimal timing occurs at TR=3.0 s and PID =1.4 s when the arterial compartment is perfectly suppressed.

FMRI results

Activation maps (thresholded at Z>3, or p<0.0013) from a representative subject collected with the PCASL sequence (TR = 4 sec) and with the VSI sequence (TR= 4sec) are shown in Fig. 8 overlaid on their corresponding perfusion weighted image (expressed as percent signal change between velocity selective and non-selective scans). The cases for TR=3 and 2 sec. are shown in supporting figure S.5. It is clear from the figure that VSI pulses produced larger % signal changes than the PCASL images for our chosen timing parameters, approximated from the simulations on Fig. 7. Table 2 show the temporal and spatial SNR of the VSI acquisitions, as well as the number of active voxels and the mean Z score of the active region (all quantities are expressed as a fraction relative to PCASL). The measures are expressed as a fraction relative to the PCASL case. Generally, the performance of VSI pulses was comparable to that of PCASL pulses at the same TR, except for subject #3, where PCASL outperformed VSI. However, the temporal SNR of the VSI pulse sequence was significantly larger (more than twice as much). When TR was reduced, VSI pulses outperformed the PCASL sequence. More specifically, the

perfusion weighted images collected using the VSI labeling scheme showed significant improvement in temporal SNR relative to PCASL, and increased the Z scores in the active regions significantly. However, the table also shows that the spatial resolution and the number of voxels activated did not increase significantly in any of the VSI acquisitions. We observed that, when the post inversion delay was reduced to 1.2 sec (TR=2 s), significant contribution from the vasculature was evident in the images. ASL images collected with the VSI sequence using a TR of 2 s failed to produce quality maps in subject #1, and was excluded from the analysis.

Discussion

The VSI sequence with careful choice of pulse sequence timing parameters, has superior SNR relative to PCASL because VSI pulses nearly eliminate the transit time from the application of the label and its arrival at the tissue. This reduces the loss of label from longitudinal relaxation quite significantly. Hence, VSI pulses are particularly well suited for white matter perfusion imaging, given the longer bolus arrival times of the white matter.

The kinetics of the VSI input function conforms to the standard two-compartment model and can be used to estimate important hemodynamic parameters. The fit to the model confirms the expected features of the technique and reveals important information about the input function. For example, short bolus arrival delays were observed in grey or white matter (less than half a second). We note that the bolus arrival time in white matter is longer than for grey matter, which is not unexpected, given the shape and velocity distribution of the brain's arterial network. Importantly, however, the size of the region where the VSI pulses are effective is not entirely clear, as it will be determined by the transmit coil's profile and the linear region of the gradients. Our data indicate that our 3T GE MR750 scanner's body coil produces a region that is large enough that the "tail-end" of the VSI arterial input function was not apparent in the explored time delay range (200-2600 ms). Beyond that time, the expected T1 decay of the label in a 3 second TR is approximately 85%, so there is no need to apply crushers. However, it may be advantageous to use velocity selective saturation pulses to remove residual labeled arterial

signals for shorter post labeling delays and faster acquisitions. Future work will focus on characterizing the tail end of the arterial input function in greater detail.

There are some limitations in our modeling work that must be considered. The first is that the model includes a large number of parameters to be estimated, and we had to make some assumptions based on educated guesses in order to be able to estimate the parameters of interest. First, we assumed a Gaussian distribution of bolus arrival times at a given voxel, whose standard deviation was 100 ms. Second, we fitted the labeling efficiency from the grey matter uptake curves and assumed that value as a constant for the white matter parameter fits, instead of estimating it separately, because the white matter fits were otherwise poor due to insufficient SNR. While the inversion efficiency of the blood should be the same for both grey and white matter (the VSI pulse was the same in both cases), it would have been preferable to estimate it separately for each compartment. These assumptions are sources of uncertainty in our parameter estimates.

Whereas we estimated perfusion in the tracer kinetic experiments in the first part of the study, we did not aim at quantification of CBF in the FMRI time series. Doing so would require collecting a reference scan as a measure of spin density. In our present experiment, the observed ASL FMRI signal amplitude roughly corresponds to a relative CBF measurement, but not an absolute one.

It must be noted that in our study, we did not make use of background suppression pulses in order to eliminate confounds from the comparison between the different input functions. The timing and number of background suppression pulses need to be optimized for each technique's characteristics and post labeling delay. Thus, background suppression may not be equally effective in all techniques. However, the inversion of stationary spins inherent to the VSI method likely reduces the contribution of physiological fluctuations by reducing the contribution of stationary spins, which are not fully relaxed after the VSI pulses. Thus, the VSI pulse itself provides partial suppression of unwanted background signals.

Our FMRI study did not employ arterial suppression pulses so the observed functional signal changes are due to a mix of arterial volume and perfusion changes. We made this choice because blood volume is known to increase significantly during activation, thus increasing the sensitivity to neural activity, although this results in some loss of spatial specificity, similar to vascular effects in the BOLD signal. We note that if greater specificity were needed, the arterial suppression pulses could indeed be included.

Given the features of the VSI's arterial input function, we observed that VSI pulses offer comparable SNR to PCASL for standard perfusion images, in line with previous findings. VSI timing parameters were chosen based on measurements of the label uptake curves, and on the above simulations (see Figs. 6 and 7). It is important to note that the SNR would be higher with a much shorter post labeling delay (< 800 ms), but those images would be dominated by the arterial compartment. Our simulations indicate that in order to measure the perfusion rate in the tissue, a longer delay is needed (>1200 ms).

We did not consider shorter timing parameters for PCASL, because that case has already been explored in the literature, as in the case of the AVAST technique (28–30)

Another attractive feature of these particular VSI pulses with spin-echo refocusing is that they do not require off-resonance correction as in the case of PCASL (26,31). As noted by Qin et al., and in our own experience here, VSI pulses are robust to B1 and B0 imperfections but require calibration of the B1 pulse.

VSI permits reduction of TR, which in turn allows for faster sampling of the perfusion time series, and thus more data collected in the same amount of time, which leads to further SNR efficiency and sensitivity gains. When the post labeling delay is reduced along with TR, the contribution of the vasculature to the ASL signal increases, but this also increases the sensitivity to brain activity, consistent with previous work (28–30). However, we find that as TR gets

shorter than 3 seconds, the SNR did not improve in all subjects. This is most likely because the label may not have cleared the region completely between the label and control scans in cases where flow velocity in the arteries is slower, or the arterial network is more tortuous and the spins have a greater distance to travel. Our uptake curves suggest that the input function was longer than 2 seconds, in which case, some of the spins may be labeled twice when the TR was 2 seconds, which would muddle the quantification process and could potentially yield erroneous results. We hypothesize that this effect may be responsible for some of the spurious activation clusters in the figure.

A challenge with VSI-ASL is the presence of eddy current effects. As seen in Supporting Figure S6, our own phantom experiments show larger eddy current effects than those reported previously by Qin et al. The eddy current artefacts observed on the edges of the phantom can reach 1% signal change or higher, which is problematic when the ASL signal itself is in that range. In this regard, there are three important observations to note. First, these artefacts correspond to scalp regions, rather than on the cortices, where the eddy current artefacts are much smaller. Secondly, the eddy current effects will bias the perfusion measurement, so perfusion values near the edges of the brain may be inflated. However, the bias from eddy currents does not interfere with the signal increases of interest in an FMRI experiment. Having said that, these eddy current artefacts are indeed a challenge for this technique that will require further development.

In summary, we have characterized the tracer kinetics of VSI pulses in order to design a perfusion based FMRI pulse sequence. Our data show that VSI-ASL is less sensitive to bolus arrival time effects, relative to PCASL. Additionally, it allows for faster temporal resolution, which can in turn be leveraged to achieve greater temporal SNR and increased sensitivity to perfusion changes due to activation.

Acknowledgements

National Institutes of Health (R21EB021562)

Figure Captions

Figure 1. Schematic diagram of an ASL sequence employing Velocity Selective Inversion pulses for labeling. Optional vascular suppression consisting of BIR-8 Velocity Selective Saturation pulses can be included immediately before acquisition. Image acquisition is carried out using 3D stack of spirals.

Figure 2. Bloch simulated magnetization for both arterial and extravascular compartments after a VSI pulse, based on Eqs. [1-4]. . On the top, a non-selective pulse inverts the magnetization in both moving (vascular) and quasi-stationary (extravascular) spins. The middle panel shows the velocity selective case, in which only the quasi-stationary (extravascular) spins are inverted. Finally, the bottom panel shows the observed difference between the observed signals in the velocity selective and non-selective cases as a function of time after the pulse is applied. If magnitude-only images are used, as is routine in MR imaging, one should observe a sign reversal in the early part of the curve.

Figure 3. Subtraction images collected at different times after the application of a VSI pulse. The images are computed as % signal difference between selective and non-selective cases, relative to a reference image without any preparation pulses. Each column shows four slices from the collected volume. Each row represents a single slice collected at different post inversion delays. The images were acquired without using vascular suppression. Supporting Figure S4 shows the results from the same experiment using a BIR-8 velocity selective saturation pulse for vascular suppression. These results are consistent with Fig. 2.

Figure 4. Percent signal change observed after a delay following the application of a VSI pulse (see Fig. 3). These time courses were extracted from grey and white matter regions separately and averaged across all participants.

Figure 5. Model fit of the VSI kinetic function to the observed experimental data for each subject, indicating good agreement between the two.

Figure 6. Bloch equation simulation of the evolution of the longitudinal magnetization in a perfusion based FMRI experiment using VSI pulses. No perfusion changes were simulated in this segment.

Figure 7. Optimization of the VSI pulse sequence for FMRI. The top two panels show the simulated percent signal change observed without (left) and with (right) arterial suppression over a range of combinations of TR and Post Inversion Delay. The bottom two panels show the theoretical SNR of the measurement, by scaling the ASL signal by the square root of the number of images that can be collected in that unit of time for each combination of parameters. (Note the black region on the bottom left corner of the plots. Those combinations of TR and PID are not realizable, so they are set to zero in the plot).

Figure 8. Activation maps from a representative subject overlaid on the mean perfusion image for FMRI experiments conducted using the PCASL sequence (for reference) and the VSI sequence using TR=4. The cases where TR was shortened to 3 and 2 sec. are shown in supporting figure S.5.

Supporting information

Supporting Information Figure S1. Velocity selective inversion pulse. The velocity selective gradient (played along the z-axis) can be seen in the top panel. The middle panel shows the amplitude of the RF pulse, which consists of nine short pulses (20 degree flip), interspersed with pairs of larger 180 degree hard pulses. The bottom panel shows the phase of the RF pulse.

Supporting Information Figure S2. Diagram of the BIR-8 velocity selective saturation pulses proposed in (18,19).

Supporting Information Figure S3. Velocity Profiles for the velocity selective inversion pulse used for labeling (left panel), and for the velocity selective saturation pulse used for arterial suppression (right panel).
The first zero-crossing for the velocity saturation pulse happens at 0.7 cm/s . The efficiency of the velocity selective inversion pulse varies with velocity. According to this simulation, the mean labeling efficiency (defined as the magnetization difference between velocity selective and non-selective cases, relative to the relaxed magnetization) is 84% for the range between 5 and 80 cm/s.

Supporting Information Figure S4. Subtraction images collected at different times after the application of a VSI pulse. The images are computed as % signal difference between selective and non-selective cases, relative to a reference image without any preparation pulses. Each column shows four slices from the collected volume. Each row represents a single slice collected at different post inversion delays. The images were acquired with using using a BIR-8 velocity selective saturation pulse for vascular suppression. These results are consistent with Fig. 2.

Supporting Information Figure S5. Activation maps from a representative subject overlaid on the mean perfusion image for FMRI experiments conducted the VSI sequence using TR of 3 and 2 sec.

Supporting Information Figure S6. Eddy current tests carried out on an Agar phantom. Some differences in magnitude and phase are detected between the velocity selective and the non-selective cases. As expected, these differences decay with the post inversion delay, but

contribute to the error in the early times of the uptake curve, primarily on the edges of the head.

Table 1: Hemodynamic parameter fits from the curves shown in figure 5

White Matter				Grey Matter			
Inversion Efficiency(%)	CBVa (%)	Perfusion (ml/min/100g)	BAT (ms)	Inversion Efficiency (%)	CBVa(%)	Perfusion (ml/min/100g)	BAT (ms)
59	0.28	30.8	394	69	0.58	33.2	100
59	0.50	34.4	376	50	1.8	76.1	62.6
59	0.37	44.7	383	50	1.8	117.4	50.0
59	0.53	32.0	396	70	0.73	36	99.5
59	0.57	30.0	194	59	1.3	41	65.5
59 *	0.45 +/- 0.11	34.4 +/- 5.4	349 +/- 77.5	59 +/ 8.8	1.2 +/- 0.52	60.8 +/- 32	75.6 +/- 20.6

Table 2: Activation results obtained from VSI sequences, expressed as a fraction relative to PCASL. (Mean +/- standard deviation over subjects). The significance of the difference was assessed as the p-value of a paired t-test of the difference between each acquisition and PCASL. Asterisks indicate that the difference is statistically significant at p< 0.05.

	TR = 4000	**TR=3000**	**TR = 2000**
Temporal SNR	2.50 +/- 1.36 P=0.0182 *	2.43 +/- 1.07 P=0.0416 *	3.41 +/- 1.47 P=0.0005 *
Spatial SNR	1.11 +/- 0.48 P=0.9292	1.24 +/- 0.66 0.2998	1.36 +/- 0.70 0.4497

Number of Active Voxels (Z>3)	1.29 +/1.19 P=0.7390	2.81 +/- 2.48 P=0.5737	4.29 +/- 2.87 P=0.1583
Average Z score in commonly activated region	1.04 +/- 0.17 P=0.037 *	1.31 +/- 0.25 P=0.0035 *	1.59 +/- 1.16 P=0.0049 *

References

1. Alsop DC, Detre JA, Golay X, et al. Recommended implementation of arterial spin-labeled Perfusion mri for clinical applications: A consensus of the ISMRM Perfusion Study group and the European consortium for ASL in dementia. Magn. Reson. Med. 2015;73. doi: 10.1002/mrm.25197.

2. Aguirre GK, Detre J a, Zarahn E, Alsop DC. Experimental design and the relative sensitivity of BOLD and perfusion fMRI. Neuroimage [Internet] 2002;15:488–500. doi: 10.1006/nimg.2001.0990.

3. Aguirre GK, Detre J a., Wang J. Perfusion fMRI for Functional Neuroimaging. Int. Rev. Neurobiol. [Internet] 2005;66:213–236. doi: 10.1016/S0074-7742(05)66007-2.

4. Aguirre GK, Detre J a. The development and future of perfusion fMRI for dynamic imaging of human brain activity. Neuroimage [Internet] 2012;62:1279–1285. doi: 10.1016/j.neuroimage.2012.04.039.

5. Buch S, Ye Y, Haacke EM. Quantifying the changes in oxygen extraction fraction and cerebral activity caused by caffeine and acetazolamide. J. Cereb. Blood Flow Metab. 2016:0271678X16641129. doi: 10.1177/0271678X16641129.

6. Pauls MMH, Clarke N, Trippier S, Betteridge S, Howe FA, Khan U, Kruuse C, Madigan JB, Moynihan B, Pereira AC. Perfusion by Arterial Spin labelling following Single dose Tadalafil In Small vessel disease (PASTIS): study protocol for a randomised controlled trial. Trials 2017;18:229.

7. Hshieh TT, Dai W, Cavallari M, et al. Cerebral blood flow MRI in the nondemented elderly is not predictive of post-operative delirium but is correlated with cognitive performance. J. Cereb. Blood Flow Metab. [Internet] 2017;37:1386–1397. doi: 10.1177/0271678X16656014.

8. Demeter E, Hernandez-Garcia L, Sarter M, Lustig C. Challenges to attention: A continuous arterial spin labeling (ASL) study of the effects of distraction on sustained attention. Neuroimage 2011;54:1518–1529. doi: 10.1016/j.neuroimage.2010.09.026.
9. Norris DG, Schwarzbauer C. Velocity selective radiofrequency pulse trains. J. Magn. Reson. 1999;137:231–236. doi: 10.1006/jmre.1998.1690.
10. Wong EC, Cronin M, Wu W-C, Inglis B, Frank LR, Liu TT. Velocity-selective arterial spin labeling. Magn. Reson. Med. [Internet] 2006;55:1334–1341. doi: 10.1002/mrm.20906.
11. Wu W-C, Wong EC. Feasibility of velocity selective arterial spin labeling in functional MRI. J. Cereb. Blood Flow Metab. [Internet] 2007;27:831–838. doi: 10.1038/sj.jcbfm.9600386.
12. Schmid S, Heijtel DFR, Mutsaerts HJMM, Boellaard R, Lammertsma A a, Nederveen AJ, Osch MJP Van. Comparison of velocity and acceleration selective arterial spin labeling with 15 O H 2 O positron emission tomography. 2014;32:4056. doi: 10.1038/jcbfm.2015.42.
13. Schmid S, Ghariq E, Teeuwisse WM, Webb A, Van Osch MJP. Acceleration-selective arterial spin labeling. Magn. Reson. Med. 2014;71:191–199. doi: 10.1002/mrm.24650.
14. Qin Q, van Zijl PCM. Velocity-selective-inversion prepared arterial spin labeling. Magn. Reson. Med. [Internet] 2016;76:1136–1148. doi: 10.1002/mrm.26010.
15. Qin Q, Van Zijl PCM. Velocity-Selective Inversion Prepared Arterial Spin Labeling for 3D Whole-Brain Perfusion Measurement. In: Proc. Intl. Soc. Mag. Res. Med. Milan; 2014. p. 420.
16. Nielsen JF, Hernandez-Garcia L. Functional perfusion imaging using pseudocontinuous arterial spin labeling with low-flip-angle segmented 3D spiral readouts. Magn. Reson. Med. [Internet] 2013;69:382–390. doi: 10.1002/mrm.24261.
17. Levitt MH, Freeman R, Frenkiel T. Broadband Decoupling in High-Resolution Nuclear Magnetic Resonance Spectroscopy. Adv. Magn. Opt. Reson. 1983;11:47–110. doi: 10.1016/B978-0-12-025511-5.50008-6.
18. Meakin J a., Jezzard P. An optimized velocity selective arterial spin labeling module with reduced eddy current sensitivity for improved perfusion quantification. Magn. Reson. Med. [Internet] 2013;69:832–838. doi: 10.1002/mrm.24302.
19. Guo J, Meakin J a., Jezzard P, Wong EC. An optimized design to reduce eddy current sensitivity in velocity-selective arterial spin labeling using symmetric BIR-8 pulses. Magn. Reson.

Med. [Internet] 2014;73:1085–1094. doi: 10.1002/mrm.25227.
20. Qin Q, Grgac K, Van Zijl PCM. Determination of whole-brain oxygen extraction fractions by fast measurement of blood T2 in the jugular vein. Magn. Reson. Med. 2011;65:471–479. doi: 10.1002/mrm.22556.
21. Williams DS, Detre J a, Leigh JS, Koretsky a P. Magnetic resonance imaging of perfusion using spin inversion of arterial water. Proc. Natl. Acad. Sci. U. S. A. [Internet] 1992;89:212–216. doi: 10.1073/pnas.89.9.4220e.
22. Detre J a, Leigh JS, Williams DS, Koretsky a P. Perfusion imaging. Magn. Reson. Med. [Internet] 1992;23:37–45. doi: 10.1002/mrm.1910230106.
23. Lu H, Clingman C, Golay X, van Zijl PCM. Determining the longitudinal relaxation time (T1) of blood at 3.0 Tesla. Magn. Reson. Med. [Internet] 2004;52:679–682. doi: 10.1002/mrm.20178.
24. Qin Q, Shin T, Schär M, Guo H, Chen H, Qiao Y. Velocity-selective magnetization-prepared non-contrast-enhanced cerebral MR angiography at 3 tesla: Improved immunity to b0/b1 inhomogeneity. Magn. Reson. Med. [Internet] 2015;0:n/a-n/a. doi: 10.1002/mrm.25764.
25. Glover BGH. FBIRN Stability phantom QA procedures : 2005:1–6.
26. Jahanian H, Noll DC, Hernandez-Garcia L. B 0 field inhomogeneity considerations in pseudo-continuous arterial spin labeling (pCASL): Effects on tagging efficiency and correction strategy. NMR Biomed. [Internet] 2011;24:1202–1209. doi: 10.1002/nbm.1675.
27. Restom K, Behzadi Y, Liu TT. Physiological noise reduction for arterial spin labeling functional MRI. Neuroimage [Internet] 2006;31:1104–1115. doi: 10.1016/j.neuroimage.2006.01.026.
28. Jahanian H, Peltier S, Noll DC, Garcia LH. Arterial cerebral blood volume-weighted functional MRI using pseudocontinuous arterial spin tagging (AVAST). Magn. Reson. Med. 2015;73. doi: 10.1002/mrm.25220.
29. Liu P, Dimitrov I, Andrews T, et al. Multisite evaluations of a T2-relaxation-under-spin-tagging (TRUST) MRI technique to measure brain oxygenation. Magn. Reson. Med. 2016;75:680–687. doi: 10.1002/mrm.25627.
30. Shah YS, Hernandez-Garcia L, Jahanian H, Peltier SJ. Support vector machine classification of arterial volume-weighted arterial spin tagging images. Brain Behav. 2016;6. doi:

10.1002/brb3.549.

31. Luh WM, Talagala SL, Li TQ, Bandettini P a. Pseudo-continuous arterial spin labeling at 7 T for human brain: Estimation and correction for off-resonance effects using a Prescan. Magn. Reson. Med. [Internet] 2013;69:402–410. doi: 10.1002/mrm.24266.

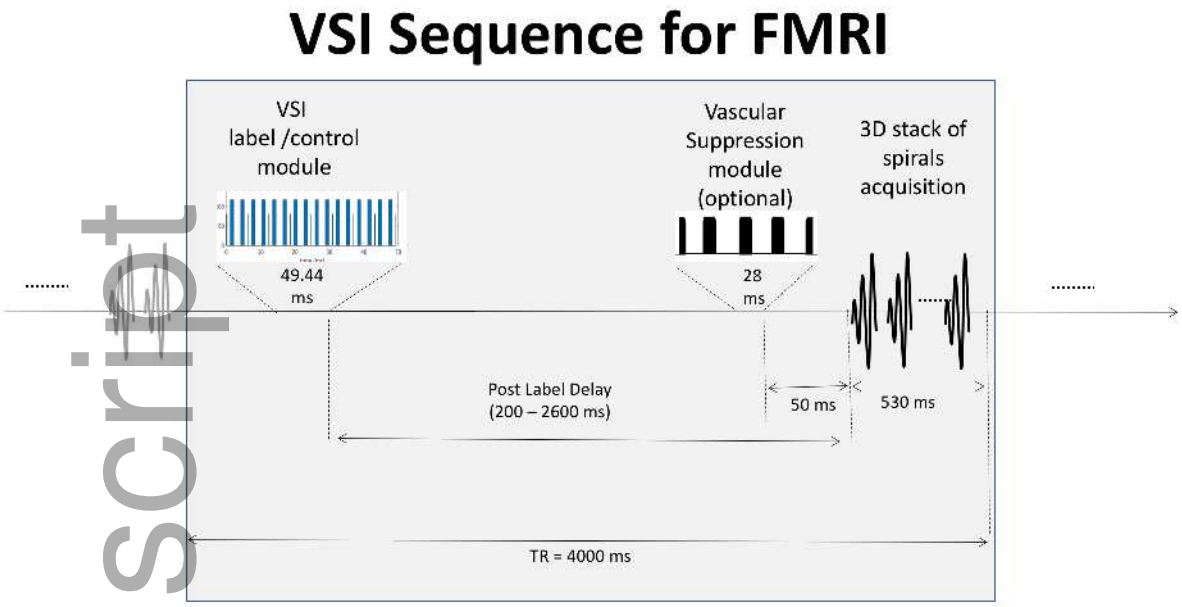

mrm_27461_f1.tiff

Simulated Longitudinal Magnetization in VSI experiment

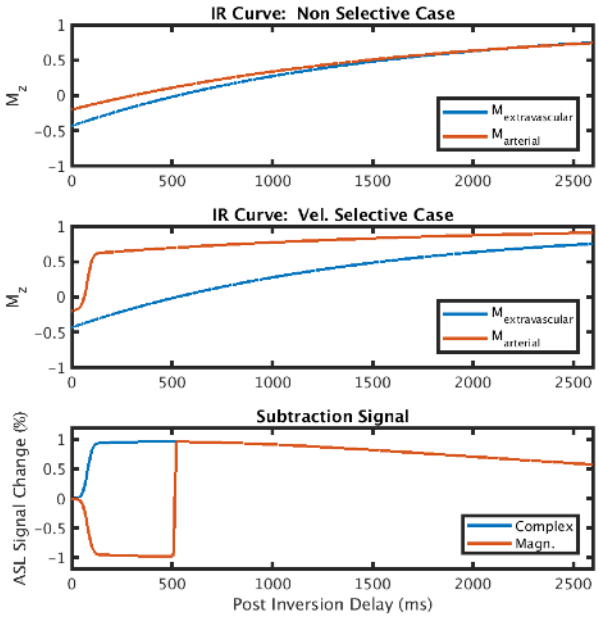

mrm_27461_f2.tiff

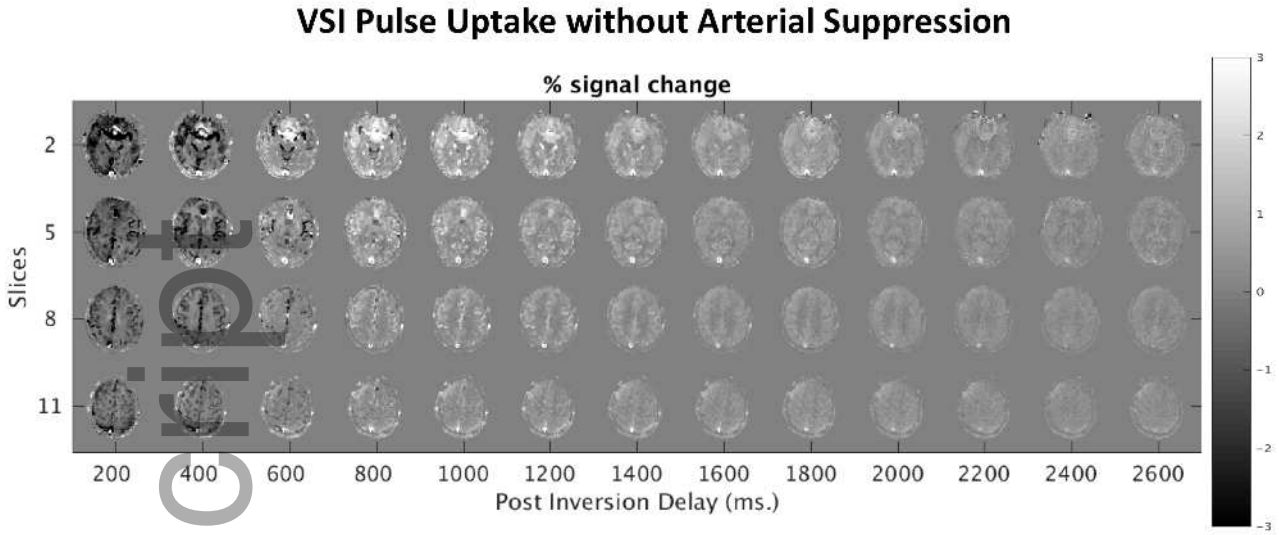

mrm_27461_f3.tiff

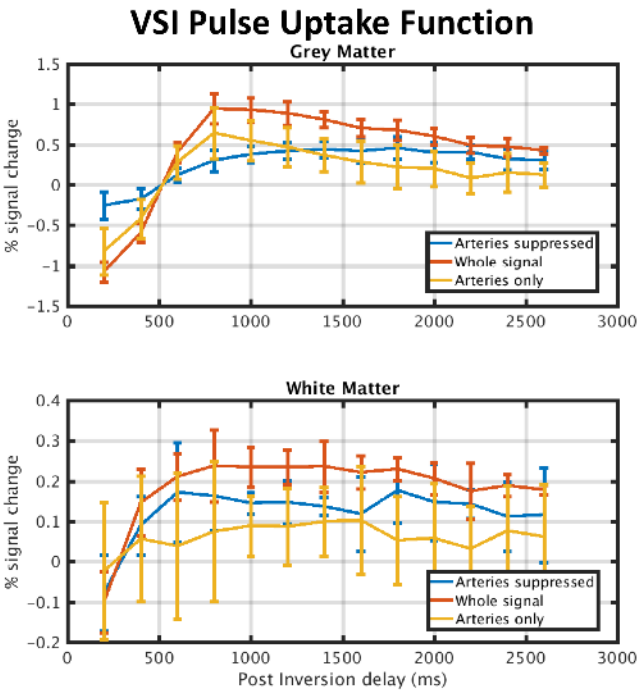

mrm_27461_f4.tiff

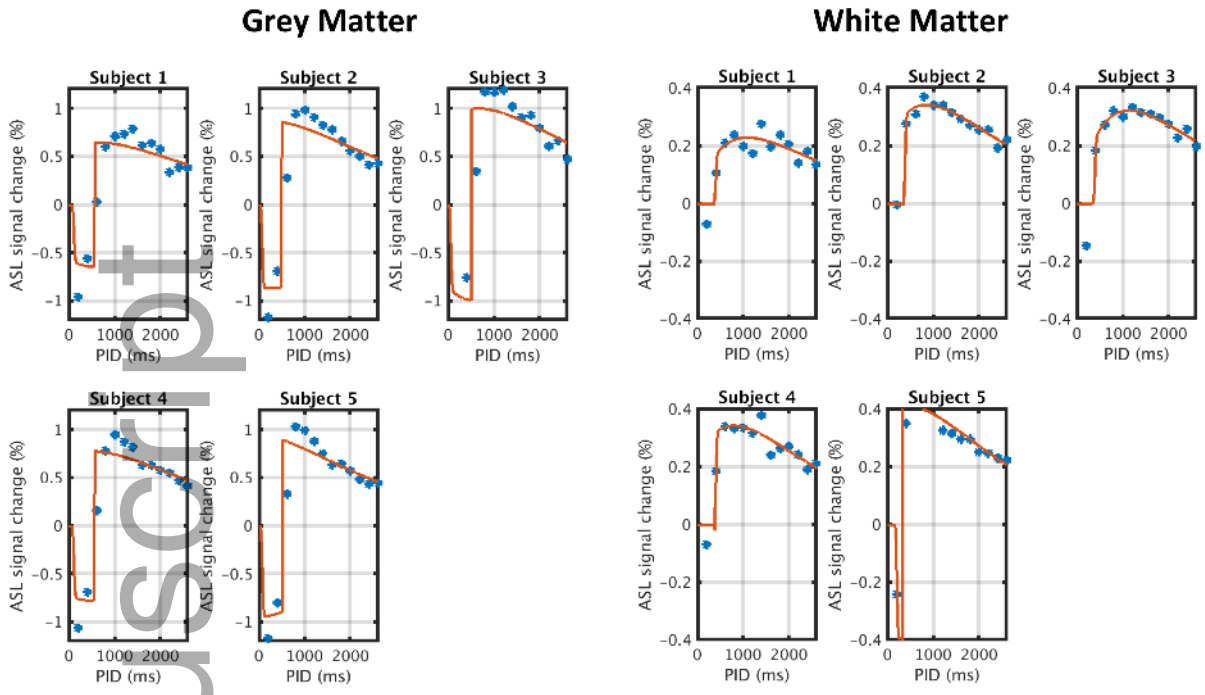

mrm_27461_f5.tiff

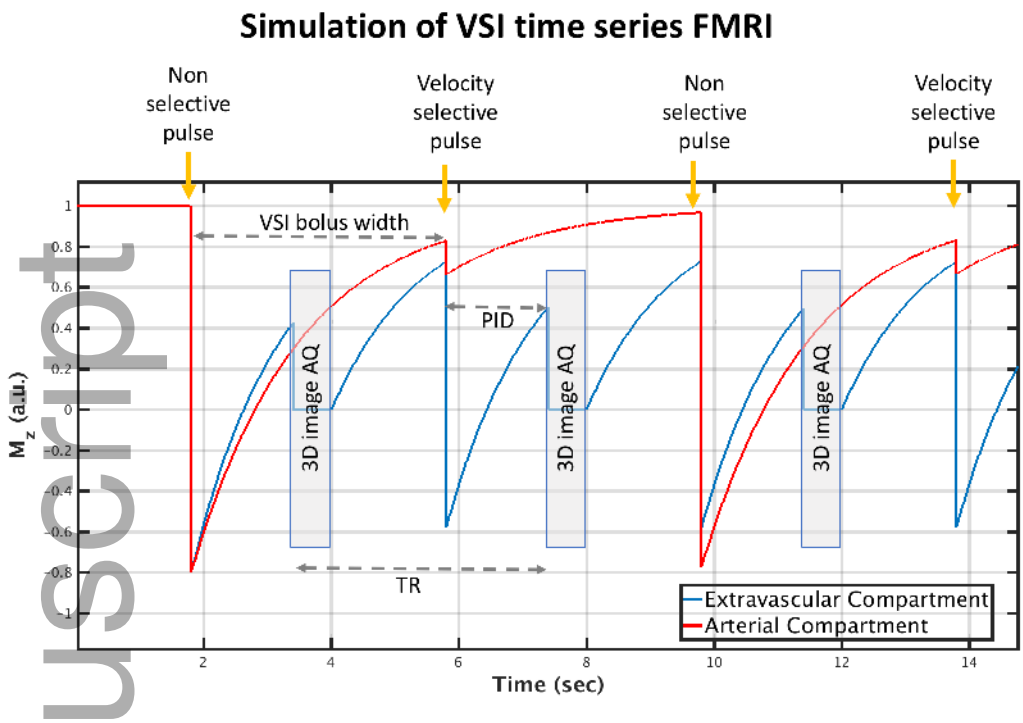

mrm_27461_f6.tiff

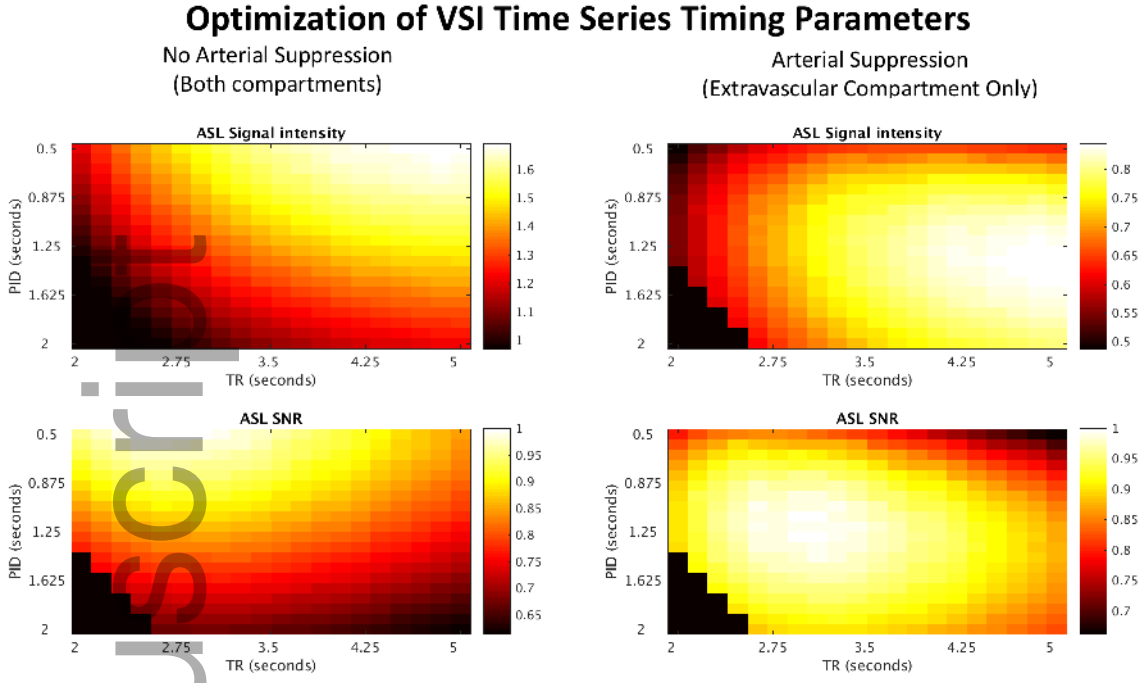

mrm_27461_f7.tiff

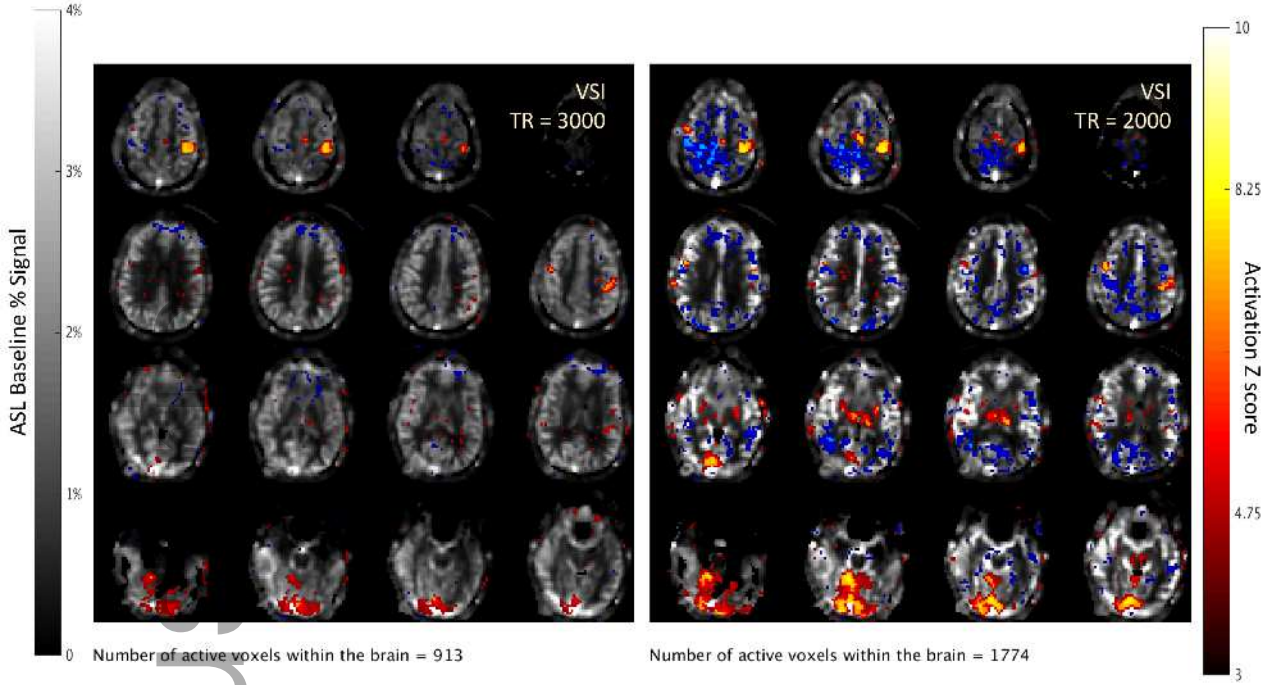

mrm_27461_f8.tiff